

## Development of Machine-Learning Potential for Sodium Combustion Simulations: Tests for Basic Properties of Liquid Na, Solid Na<sub>2</sub>O, and Interfaces

Chae-yeong Kim, Takuju Oda\*

Department of nuclear engineering, Seoul National Univ., 1 Gwanak-ro, Gwanak-gu, Seoul 08826

\*Corresponding author: oda@snu.ac.kr

### 1. Introduction

Liquid sodium is used as a coolant in sodium-cooled fast reactor (SFR), because it has good thermal properties as a heat transfer fluid, low neutron absorption cross section, and good compatibility with structural materials. One of the key engineering challenges in the development of SFR is the sodium fire with air. The fire brings not merely engineering safety issues but also a social issue in terms of the public acceptance of SFR. For appropriate control and mitigation of sodium fire, comprehensive and detailed understanding of its processes is vital. However, existing codes for sodium fire evaluation largely simplify complex chemical reactions involved in the combustion, which may limit their transferability and prediction accuracy.

Molecular dynamics (MD) is expected to greatly enhance the understanding of combustion processes because it can address reaction dynamics in the atomic scale. To perform MD simulations, an accurate potential model must first be prepared. However, no potential model has been reported to date that can be applied to sodium combustion phenomena. This is mainly because sodium combustion is a complex multi-physics phenomenon involving liquid Na, solid Na<sub>2</sub>O, gas molecules and their interfaces, and it is difficult to construct an accurate potential model using empirical methods.

Therefore, in the present study, machine learning is applied in the development of a potential model. As the first step toward MD simulations of sodium combustion, we constructed and tested a machine-learning potential model for basic properties of liquid Na, solid Na<sub>2</sub>O and their interfaces. The calculated properties were validated in comparison with experimental data and first-principles calculation results.

### 2. Methods

#### 2.1. Moment Tensor Potentials (MTP)

In general, a machine learning potential is constructed to reproduce energy, force and stress data obtained from DFT calculations. Among several proposed machine learning models, Moment Tensor Potential (MTP) [1] was selected. MTP has a flexible functional form and is expected to simultaneously reproduce DFT data of both metals (Na) and insulators (Na<sub>2</sub>O, etc), which are chemically different.

MTP is composed of radial and angular functions. For the radial functions, the minimum and maximum cutoff distances of radial basis functions were set as 1.35 Å and

6 Å, respectively. The number of angular basis functions used in MTP is controlled by one parameter called *level* [1]. An MTP model of a higher level holds more basis functions and thus is generally more accurate, but at a higher computational cost. To determine the best balance between accuracy and speed, MTPs of four different levels, 12, 14, 16 and 18, were compared. Since a non-linear iterative method is used in the construction of MTP, the quality of MTP depends on the initial parameters characterized by a random seed. Thus, five MTPs were generated with different seed numbers for each level to compare the performance. **Figure 1** shows the root mean square error (RMSE) and averaged absolute error in the energy fitting with respect to the level. Above level 16, the RMSE becomes less than 2.3 meV/atom and the standard error in the energy errors of 5 cases is significantly reduced. Therefore, considering the computational cost and accuracy, 16 level was considered as the optimal setting for our research.

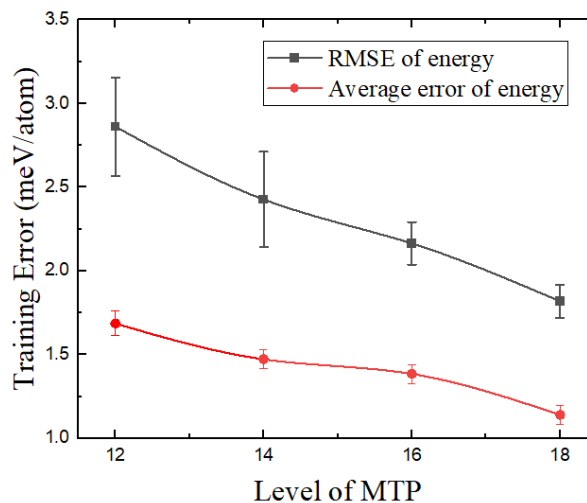


Figure 1. RMSE and average fitting error of energy with respect to maximal level of MTP

#### 2.2. DFT calculation

DFT calculations were performed to obtain energies, forces and stresses for the use in the MTP training. To reproduce the basic properties, the training reference data include the information on liquid pure Na, liquid Na with O impurity, crystal Na<sub>2</sub>O, liquid Na<sub>2</sub>O, and interfaces between Na<sub>2</sub>O and liquid Na.

All DFT calculations were conducted using the Vienna Ab initio Simulation Package (VASP) [2] based on density functional theory (DFT). For exchange-correlation functionals, Perdew-Burke-Emzerhof (PBE)

functional [3] of generalized gradient approximation (GGA) [4] was utilized. For Na and O, a  $3s^1$  electron and  $2s^2 2p^4$  electrons were considered as the valence electrons, respectively. The electronic wave functions of the valence electrons were described by plane waves with an energy cutoff of 400 eV. The effects of core electrons were modeled by using the projector augmented wave (PAW) potential method. For Na systems, first-principles molecular dynamics (FPMD) calculations were performed with an energy cutoff of 400 eV. The band energy was sampled over  $2 \times 2 \times 2$  Monkhorst-Pack grid [5] with the Methfessel-Paxton smearing scheme [6] of 0.2 eV smearing width. For  $\text{Na}_2\text{O}$  systems, the plane-wave energy cutoff was set as 400 eV and  $3 \times 3 \times 3$  gamma-centered sampling was utilized with the gaussian smearing method of 0.05 eV smearing width.

### 2.3. Potential Model Validation

The performance of the constructed MTP model was tested with respect to (1) physical properties of liquid Na, (2) physical properties of solid  $\text{Na}_2\text{O}$  crystals, and (3) interface properties between liquid Na and solid  $\text{Na}_2\text{O}$ . For this purpose, MD simulations were performed using Large-Scale Atomic/Molecular Massively Parallel Simulator (LAMMPS).[7]

For (1), the density, isothermal compressibility and radial distribution function (RDF) of liquid sodium were calculated. The density was obtained from 400 K to 1000 K, by averaging the volumes of 20 NPT simulations. RDFs at 600 K and 1000 K were obtained by NVT simulations after 10 ps equilibrium run. The isothermal compressibility was calculated from 473 K to 973 K, and the mean and variance of the volume were calculated with 5 samples of NPT simulations. Each simulation was performed for 50 ps with 1 fs time step and 102 Na atoms.

For (2), the lattice constant, bulk modulus, and elastic constant of  $\text{Na}_2\text{O}$  at 0 K were calculated by conjugate gradient (CG) method. The bulk modulus was calculated from the relation between energy and volume.

For (3), the integrity of the interfaces between liquid sodium and (100), (110) or (111) surface of crystal  $\text{Na}_2\text{O}$  was confirmed by atomic visualization after an NPT simulation. The simulations was performed for 100 ps with 1 fs time step. The target temperature and pressure were set as 600 K and 1 bar, respectively. 888 Na and 192 O atoms, 888 Na and 168 O atoms, and 1080 Na atoms and 216 O atoms were used for the interfaces with (110), (110) and (111) surfaces of crystal  $\text{Na}_2\text{O}$ , respectively.

In addition, the solution enthalpy of solid  $\text{Na}_2\text{O}$  in liquid Na was calculated in 400-1000 K from the enthalpies of solid  $\text{Na}_2\text{O}$  system (Na216O108), pure liquid Na system (Na102), and liquid Na system with an O impurity (Na101O1). To ensure statistical accuracy, the average enthalpies of liquid Na and crystalline  $\text{Na}_2\text{O}$  were calculated from NPT simulations of 20 and 5 samples, respectively. Each simulation was performed for 50 ps with 1 fs time step.

## 3. Result & Discussion

### 3.1. Liquid Na

**Figure 2** compares the temperature dependence of liquid Na density calculated by MTP with several available experimental data. Although the difference becomes larger at relatively low and high temperatures, the MTP can reasonably describe the thermal expansion from 400 K to 1000 K with a maximum error of 2% in the density.

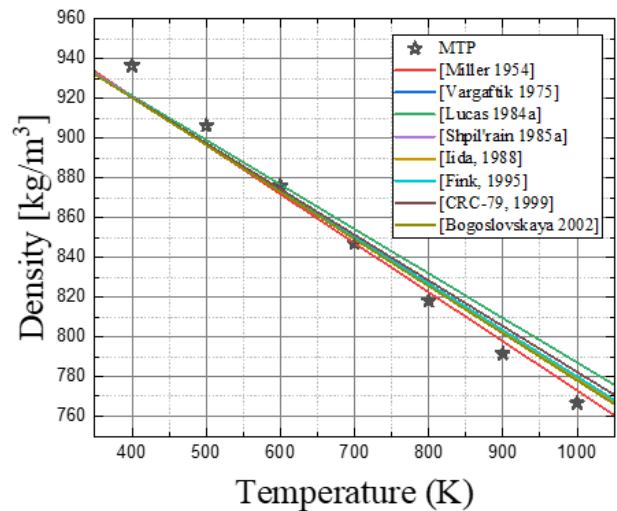


Figure 2. Comparison of calculated liquid sodium density with experimental data [8]

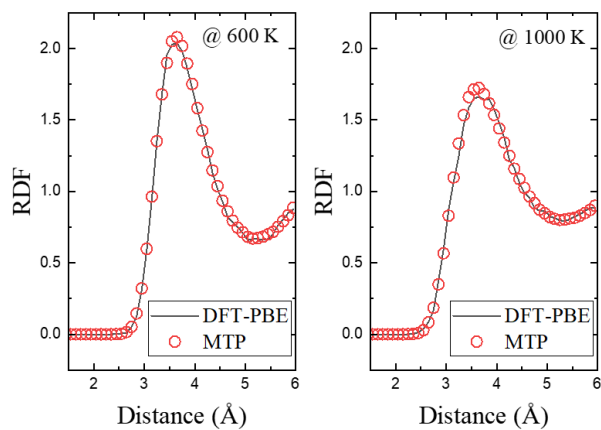


Figure 3. Radial distribution functions of liquid Na at 600 K and 1000 K

**Figure 3** shows that MTP can reproduce the RDF of the DFT calculation at both 600 K and 1000 K. The isothermal compressibility was calculated from 473 K to 1073K and compared with experimental results [9] in **Figure 4**. MTP reasonably reproduces the temperature dependence of isothermal compressibility, although it systematically underestimates the experimental data by

about 20%. This systematic error is expected to partly come from the characteristics of PBE functional.

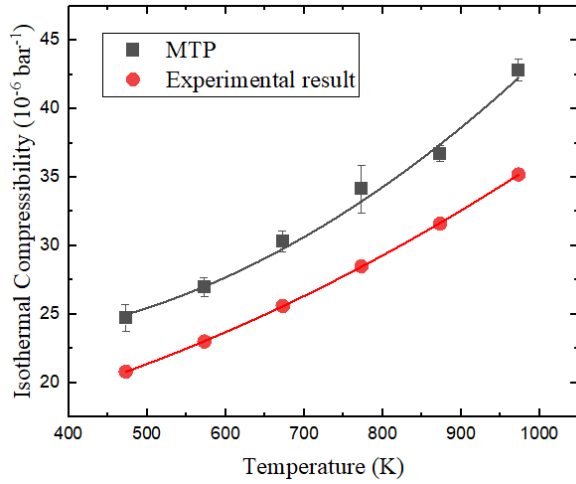


Figure 4. Comparison of isothermal compressibility between the present calculation and a previous experimental result[9]

### 3.2. Solid Na<sub>2</sub>O crystal

**Table 1** shows crystalline Na<sub>2</sub>O properties calculated by LAMMPS using the constructed MTP. The calculation results are compared with experimental and DFT calculation results. Due to a lack of experimental data, the elastic constants were only compared with DFT calculations. The elastic constants calculated by the MTP were between two DFT calculation results. In terms of bulk modulus and lattice constant, the MTP shows good agreement with the experimental data. These results demonstrate that the MTP can describe the basic physical properties of Na<sub>2</sub>O crystal reasonably.

**Table 1.** Comparison of basic properties of Na<sub>2</sub>O calculated by MTP with experimental and DFT results

	MTP	DFT-PBE [10]	DFT-PW91 [11]	Experiment
C <sub>11</sub> [GPa]	101.35	114	98.6	-
C <sub>12</sub> [GPa]	14.17	34.7	12.6	-
C <sub>22</sub> [GPa]	24.22	27.4	25.2	-
Lattice constant [Å]	5.53	5.58	5.56	5.49[12]
Bulk modulus [GPa]	48.46	54	47.04	55.6[13]

### 3.3. Interface between liquid Na and solid Na<sub>2</sub>O

Snapshots of interface simulations between liquid Na and Na<sub>2</sub>O crystals are visualized in **Figure 5**. MD simulations were performed at 600 K. The interface

structures were visually similar to those obtained from first-principles MD simulations. No numerically instabilities occurred in MD simulations using the MTP.

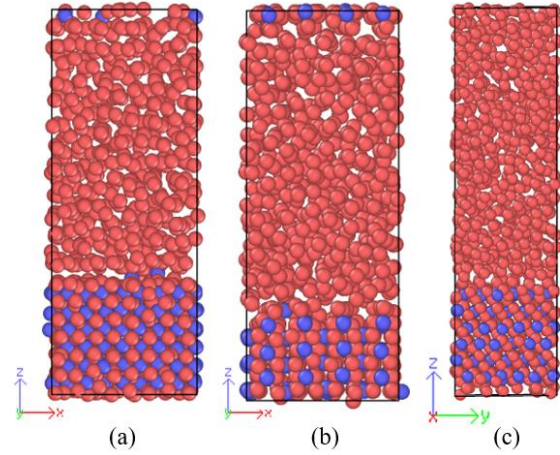


Figure 5. MD snapshots at 600 K for systems containing the interfaces between liquid Na and (a) (110), (b) (110), and (c) (111) Na<sub>2</sub>O

In **Figure 6**, the solution enthalpy calculated by MTP was compared with DFT and experimental results. The MTP correctly reproduces the solution enthalpy determined by DFT at 600K, while that at 1000 K is slightly overestimated. In the solution enthalpy calculation using DFT, the enthalpy of Na<sub>2</sub>O crystal was determined by lattice dynamics calculation using the quasi-harmonic approximation (QHA). Considering that the error in the QHA calculation at 1000 K is approximately 0.05 eV/atom [14], the agreement with DFT is reasonably good.

Comparison with the experimental data in **Figure 6** suggests that the MTP underestimates the solution enthalpy by approximately 0.1-0.2 eV. The possible reason for the error of the MTP is the overestimation in O<sub>2</sub> binding energy by DFT using the PBE functional. In a previous study, Kang et al. estimated the O-O over-binding error in various non-transition oxides to 1.33, 0.85 and 0.23 eV/O<sub>2</sub> for monoxides, peroxides and superoxides, respectively [15]. The error in the DFT calculation results used in the MTP training would have been transferred to the MTP.

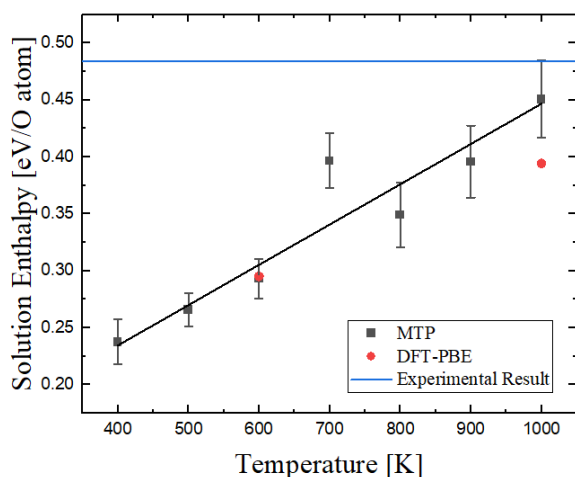


Figure 6. Comparison of  $\text{Na}_2\text{O}$  solution enthalpy in liquid Na calculated by MTP with those obtained by DFT calculation[14] and experiment[16]

#### 4. Conclusion

In this study, a machine-learning potential model was developed to reproduce the basic properties of liquid Na, crystal  $\text{Na}_2\text{O}$  and interfaces between them as the first step toward MD simulations of sodium combustion. It was confirmed that the constructed MTP model can represent the fundamental properties related to the combustion in liquid Na, solid  $\text{Na}_2\text{O}$ , and some interfaces. We plan to extend the potential model to cover other systems including  $\text{Na}_2\text{O}_2$  crystal and various Na-O gas molecules in future to realize accurate MD simulations for sodium combustion.

#### 5. Acknowledgement

This research was supported by the National Research Foundation (NRF) of Korea grant funded by the Korean government (MSIT) (No. 2021R1F1A1063748), the Brain Korea 21 FOUR Program (No. 4199990314119), and the Creative-Pioneering Researchers Program through Seoul National University.

#### REFERENCES

- [1] I. S. Novikov, K. Gubaev, E. V Podryabinkin, and A. V Shapeev, "The MLIP package: moment tensor potentials with MPI and active learning," *Mach. Learn. Sci. Technol.*, vol. 2, no. 2, p. 025002, 2021, doi: 10.1088/2632-2153/abc9fe.
- [2] J. F. G. Kresse, "Efficient iterative schemes for ab initio total-energy calculations using a plane-wave basis set," *J. Phys. Chem. B*, vol. 124, no. 20, pp. 4053–4061, 1996, doi: 10.1021/acs.jpca.0c01375.
- [3] J. P. Perdew, K. Burke, and M. Ernzerhof, "Generalized gradient approximation made simple," *Phys. Rev. Lett.*, vol. 77, no. 18, pp. 3865–3868, 1996, doi: 10.1103/PhysRevLett.77.3865.
- [4] J. P. Perdew *et al.*, "Erratum: Atoms, molecules, solids, and surfaces: Applications of the generalized gradient approximation for exchange and correlation (Physical Review B (1993) 48, 7, (4978))," *Phys. Rev. B*, vol. 48, no. 7, p. 4978, 1993, doi: 10.1103/PhysRevB.48.4978.2.
- [5] K. Hu *et al.*, "Special points for Brillouin-zone integrations," vol. 7, no. 5, pp. 5188–5192, 1976, doi: 10.1039/c8ta11250a.
- [6] M. Methfessel and A. T. Paxton, "High-precision sampling for Brillouin-zone integration in metals," *Phys. Rev. B*, vol. 40, no. 6, pp. 3616–3621, 1989, doi: 10.1103/PhysRevB.40.3616.
- [7] A. P. Thompson *et al.*, "LAMMPS - a flexible simulation tool for particle-based materials modeling at the atomic, meso, and continuum scales," *Comput. Phys. Commun.*, vol. 271, p. 108171, 2022, doi: 10.1016/j.cpc.2021.108171.
- [8] V. Sobolev, "Database of thermophysical properties of liquid metal coolants for GEN-IV," *SCK•CEN Tech. Report, SCKCEN-BLG-1069*, vol. 16, no. 12, pp. 3496–3502, 2010, [Online]. Available: [http://www.iaea.org/inis/collection/NCLCollectionStore/\\_Public/43/095/43095088.pdf](http://www.iaea.org/inis/collection/NCLCollectionStore/_Public/43/095/43095088.pdf).
- [9] A. D. Pasternak, "Isothermal compressibility of the liquid alkali metals," *Mater. Sci. Eng.*, vol. 3, no. 2, pp. 65–70, 1968, doi: 10.1016/0025-5416(68)90019-0.
- [10] M. Thompson, X. Shen, and P. B. Allen, "Density functional calculation of electronic structure and phonon spectra of  $\text{Na}_2\text{O}$ ," *Phys. Rev. B - Condens. Matter Mater. Phys.*, vol. 79, no. 11, pp. 11–13, 2009, doi: 10.1103/PhysRevB.79.113108.
- [11] T. Noinonmueng and K. Phacheerak, "Structural and Mechanical Properties of Cubic  $\text{Na}_2\text{O}$ : First-Principles Calculations ARTICLE INFO ABSTRACT," *Online) Res. J. Rajamangala Univ. Technol. Thanyaburi*, vol. 19, no. 2, pp. 2651–2289, 2020, doi: 10.14456/rj-rmтт.2020.14.
- [12] E. Zintl, A. Harder, and B. Dauth, "Lattice structure of the oxides, sulfides, selenides and tellurides of lithium, sodium and potassium," *Z. Elektrochem*, vol. 40, no. 588, p. 88, 1934.
- [13] X. Wu *et al.*, "High pressure X-ray diffraction study of sodium oxide ( $\text{Na}_2\text{O}$ ): Observations of amorphization and equation of state measurements to 15.9 GPa," *J. Alloys Compd.*, vol. 823, 2020, doi: 10.1016/j.jallcom.2020.153793.
- [14] J. Gil and T. Oda, "Solution enthalpy calculation for impurity in liquid metal by first-principles calculations: A benchmark test for oxygen impurity in liquid sodium," *J. Chem. Phys.*, vol. 152, no. 15, 2020, doi: 10.1063/1.5136324.
- [15] S. Kang, Y. Mo, S. P. Ong, and G. Ceder, "Nanoscale stabilization of sodium oxides: Implications for Na-O<sub>2</sub> batteries," *Nano Lett.*, vol. 14, no. 2, pp. 1016–1020, 2014, doi: 10.1021/nl404557w.
- [16] R. Eichelberger, "The solubility of oxygen in liquid sodium: a recommended expression," *At. Int.*, 1968.